Development of Automatic Beam-size Measurement System for KEKB

John W. FLANAGAN, Toshiyuki MITSUHASHI, and Shigenori HIRAMATSU
High Energy Accelerator Research Organization (KEK)
1-1 Oho, Tsukuba-shi, Ibaraki 305-0801, Japan

Abstract

In order to measure beam sizes at KEKB, we have installed synchrotron radiation (SR) monitors in each of the electron and positron storage rings capable of both direct imaging measurements and SR interferometry measurements. The interference pattern from the SR interferometer is digitized and analyzed using a Levenberg-Marquardt non-linear fit for precise beam-size measurement. The results are relayed back to the control room for continuous real-time measurements of the beam size, which are extremely useful for collision tuning. We here report on the data acquisition and analysis system.

1 Introduction

The KEK B-Factory is an asymmetric electron-positron collider consisting of two intersecting storage rings: the High Energy Ring (HER) for storing 8 GeV electrons, and the Low Energy Ring (LER) for storing 3.5 GeV positrons. Each ring has a complete, independent SR monitor system, consisting of a 5 mradian bend SR source magnet, water-cooled beryllium extraction mirror, closed optical beamlines and above-ground optics hutch.[1] Each beamline transports the SR beam 30-40 meters to an external optics hutch along two parallel paths. One path is used for direct imaging with adaptive optics[2], the other is used for transverse beam size measurements via SR interferometer[3] and longitudinal profile measurements via streak camera.

The focused image and the interference pattern are captured with CCD cameras in the optics hutch, and the interference pattern is analyzed by image processing software running on a computer in the hut to extract the visibility of the interference fringes. This information, along with the images themselves, are transferred to a computer in the central control room, where a monitoring program calculates the beam size from the visibility. The analysis method is described here.

2 Interference pattern analysis

The geometry of interference pattern formation is as shown in Figure 1. The SR light from the beam comes into each slit with an intensity I, assumed (and adjusted) to be equal in magnitude for each slit. The two slits have width w and are separated by a distance D, with the interference pattern being formed a distance F from the slits.

For a single-wavelength component of the incident SR, the interference pattern produced has an intensity distribution $y(x)$ of the form

$$y(x) = I_0 \left[\frac{sin(\frac{2\pi}{\lambda}Fw\Phi x)}{\frac{2\pi}{\lambda}Fw\Phi x}\right]^2 (1+\gamma cos(\frac{2\pi}{\lambda}Dx)), \quad (1)$$

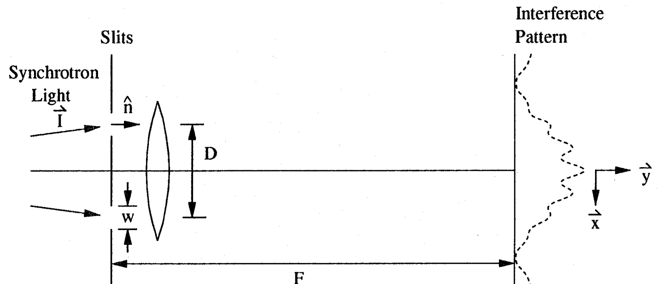

Fig. 1 Geometry of interference pattern formation.

where $I_0 \propto |\vec{I}|$ is determined by the intensity of the beam, λ is the wavelength of the light, and $\Phi \propto \vec{I}\cdot\hat{n}$ is an effective slit width correction. This represents a single-slit diffraction pattern $(sin(x)/x)^2$, in fact two single-slit patterns which are brought into overlap by the lens behind the slits, modulated by a cosine double-slit term with visibility γ determined by the spatial coherence of the SR light. The visibility is the desired quantity, from which the beam size is calculated, assuming a gaussian beam distribution and negligible source depth effects, as

$$\sigma_{beam} = \frac{\lambda L}{\pi DM}\sqrt{\frac{1}{2}\ln\frac{1}{\gamma}}, \quad (2)$$

where L is the distance from the beam source point and M is the magnification of the optical path due to, for example, curvature in the extraction mirror.

3 Functional Fit

To find the visibility γ from the interference pattern, we fit the measured pattern using the standard Levenberg-Marquardt method for non-linear fitting.[4] For this purpose, we introduce some additional terms to Equation 1 to represent a linear background, and also to correct for offsets in the origin of the image axis x, which can change as the image moves due to air fluctuations or changes in the beam orbit. Separate offsets are needed for the *sinc* and *cos* terms because small offsets in the path length to each slit from the beam will move the origin of the *cos* pattern relative to that of the *sinc* pattern. In addition, since the size of the interference pattern is adjusted using additional lenses between the slits and the CCD (not shown in Figure 1), the scales of the *sinc* and *cos* terms are taken initially as parameters.

We must also take into account the bandwidth of the light being imaged. For maximum light intensity while measuring beam sizes at low beam currents, we use bandpass filters with a fairly large FWHM of 87 nm around a center wavelength of 513 nm (Melles Griot 03 FIB 006). The effect of such a large bandwidth is to

smear the monochromatic interference pattern of Equation 1 progressively as one observes from the center of the pattern towards the edges, due to the overlapping of patterns at different characteristic scales (wavelengths). The solution is to write the fitting function as a sum over a sample of wavelengths covered by the filter, each term weighted by the transmission at that wavelength, as shown in Figure 2. The incident SR spectrum changes by only a few percent over this bandwidth, and is taken as flat.

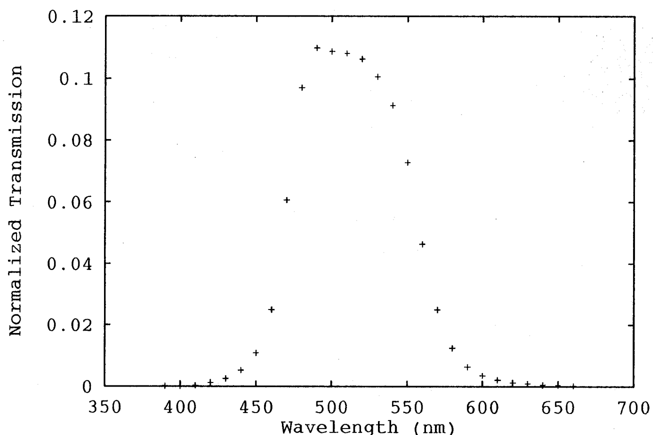

Fig. 2 Light transmission curve of SR interferometer bandpass filter. Integral under the curve is normalized to unity.

The inputs to the Marquardt algorithm are thus the fitting function,

$$y = a_1 + a_2 x + \sum_{i=1}^{n} f_i \frac{a_3}{2} \left[\frac{sin(\frac{\lambda_0}{\lambda_i} a_4 (x - a_5))}{\frac{\lambda_0}{\lambda_i} a_4 (x - a_5)} \right]^2 \times (1 + a_6 cos(\frac{\lambda_0}{\lambda_i} a_7 (x - a_8))),$$

and its partial derivatives $\partial y / \partial a_i$, needed by the algorithm for steepest-descent minimization initially and inverse-Hessian approach near the minimum. In the above equation, n is the number of wavelengths λ_i over which the filter response function f_i (with central wavelength λ_0) is sampled.

The interference pattern is digitized from CCD camera images and analyzed using a commercial image analysis package (WiT), which provides hooks for user-developed routines to be included, which is where we have installed the above procedure. The fitting module includes options to specify whether for each parameter whether it is is to be treated as free or fixed. Before fitting, a vertical smoothing filter is run over the image to reduce noise, and then the peak horizontal row is extracted. The interference pattern x axis goes along the horizontal axis in the images shown here. The vertical beam size is measured by rotating the SR light 90 degrees before reaching the slits.

Figure 3 shows the screen of the image processing computer in the optics hutch.

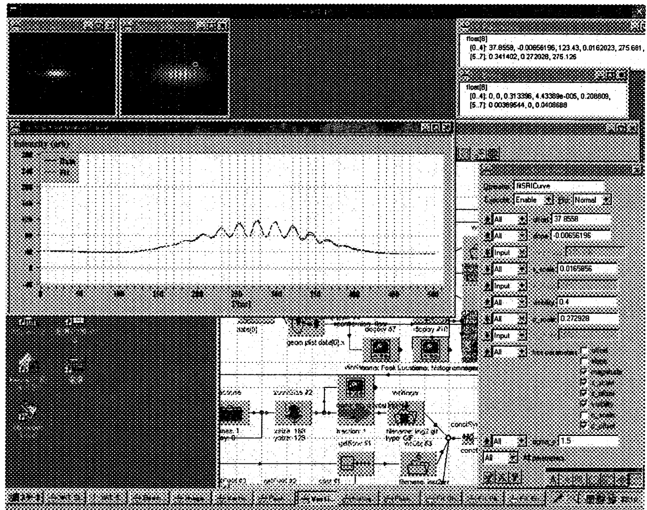

Fig. 3 Screenshot of image-processing computer in LER optics hut during image acquisition and analysis. CCD images are in upper left, the right-hand one being the interferogram. The fitting options panel is in the lower right, and the best-fit curve overlaid on data is shown in the center plot. The best-fit parameters and errors are shown in the upper right.

The bulk of the work of image analysis is thus performed on the computers in the optics hutches, with the results relayed to a computer in the control room for display and further analysis. Figures 4 and 5 show examples of the display panel in the control room in operation. The interference pattern, best fit to the extracted curve, and beam size trend graph and analysis parameters are shown in the middle row of the panel. The vertical beam size at the SR monitor source location is displayed at the top of the panel, as is the size at the interaction point calculated from the size at the SR monitor size and the beam optics parameters. Space is also reserved on the panel for horizontal beam size measurement, not yet implemented.

4 Performance

The system works quite stably once the proper starting parameters have been determined.

After adjusting the slits and camera, it is desirable to measure and fix the *cos* and *sinc* scale parameters, since they do not in principle change until the slits are changed. The offsets for the *cos* and *sinc* functions must be left free, however, due to movement of the image and variations in the optical path length from the beam to the two slits from air currents. Stability of the image is also important over the span of CCD readout ($\sim$ 20 ms).

Due to non-linearities in the CCD response at low light levels, it was attempted to leave the background fitting parameters free during operation. This works well

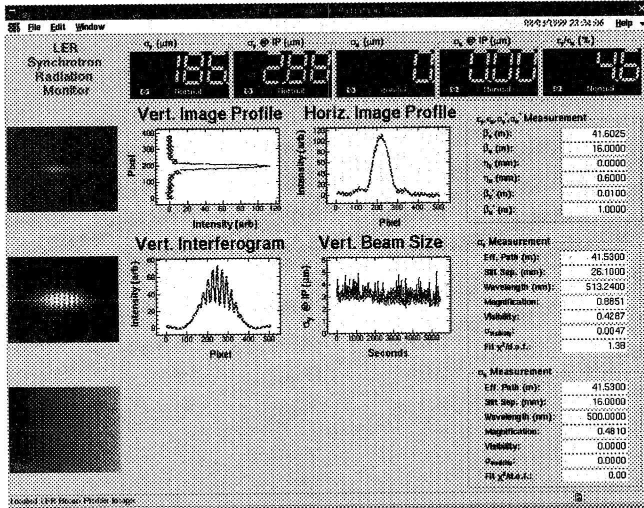

Fig. 4 SR Monitor beam-size monitoring panel in control room, showing LER vertical beam size.

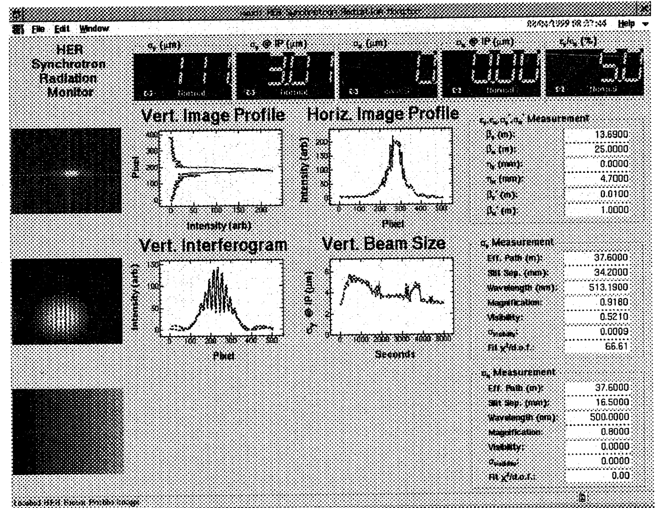

Fig. 5 SR Monitor beam-size monitoring panel in control room, showing HER vertical beam size.

at medium light levels, as long as the size of the interference pattern is adjusted to ensure that the first zeros of the *sinc* function are visible on the digitized image. However, at very low light levels (beam currents below 10-20 mA at KEKB), such freedom is more harmful than helpful due to the interaction between fitted background levels and visibility, and it was found better overall to fix the background parameters once measured.

The system will be expanded to include the continuous measurement of the curvature of the extraction mirror, and to simultaneously measure the horizontal beam size.

5 Conclusion

The online SR interferometry analysis system for the KEKB LER and HER is working well to deliver continuous, real-time measurement of the beam size via SR interferometry. Further refinements to the measurement and analysis methods are under development, as well as automation of remaining components of the final system design.

Acknowledgment

The authors are indebted to the KEKB commissioning team for their support and patience during development of the SR monitoring system, and to the support of Prof. S. Kurokawa, who has provided the leadership and support for the construction and commissioning of the synchrotron radiation monitoring system, and of KEKB.

References

[1] J.W. Flanagan, S. Hiramatsu, and T. Mitsuhashi, Proc. PAC 1999, pp. 2120-2122.

[2] N. Takeuchi et al., Tech. Digest of Nonastronomical Adaptive Optics (NAAO'97), (1997) p. 26.

[3] T. Mitsuhashi et al., Proc. EPAC 1998, p. 1565.

[4] W.H. Press, S.A. Teukolsky, W.T. Vetterling and B.P. Flannery, *Numerical Recipes in C: The Art of Scientific Computing*, Second Edition, CUP (1992) pp. 681-688.